THE JOURNAL OF BIOLOGICAL CHEMISTRY
Vol. 277, No. 25, Issue of June 21, pp. 22725–22733, 2002

Printed in U.S.A.

Structural Characterizations of Fusion Peptide Analogs of Influenza Virus Hemagglutinin

IMPLICATION OF THE NECESSITY OF A HELIX-HINGE-HELIX MOTIF IN FUSION ACTIVITY*

Received for publication, January 4, 2002, and in revised form, March 21, 2002
Published, JBC Papers in Press, April 5, 2002, DOI 10.1074/jbc.M200089200

Chun-Hua Hsu‡§, Shih-Hsiung Wu§¶‖, Ding-Kwo Chang, and Chinpan Chen‡ ‡‡**

*From the ‡Institute of Biomedical Sciences, Academia Sinica, Taipei 115, Taiwan, the ¶Institute of Biological Chemistry, Academia Sinica, Taipei 115, Taiwan, the §Institute of Biochemical Sciences, National Taiwan University, Taipei 106, Taiwan, and the **Institute of Chemistry, Academia Sinica, Taipei 115, Taiwan*

Infection by enveloped viruses initially involves membrane fusion between viral and host cell membranes. The fusion peptide plays a crucial role in triggering this reaction. To clarify how the fusion peptide exerts this specific function, we carried out biophysical studies of three fusion peptide analogs of influenza virus hemagglutinin HA2, namely E5, G13L, and L17A. E5 exhibits an activity similar to the native fusion peptide, whereas G13L and L17A, which are two point mutants of the E5 analog, possess much less fusion activity. Our CD data showed that the conformations of these three analogs in SDS micelles are pH-dependent, with higher α-helical contents at acidic pH. Tryptophan fluorescence emission experiments indicated that these three analogs insert deeper into lipid bilayers at acidic pH. The three-dimensional structure of the E5 analog in SDS micelles at pH 4.0 revealed that two segments, Leu^{2}–Glu^{11} and Trp^{14}–Ile^{18}, form amphipathic helical conformations, with Gly^{12}-Gly^{13} forming a hinge. The hydrophobic residues in the N- and C-terminal helices form a hydrophobic cluster. At neutral pH, however, the C-terminal helix of Trp^{14}–Ile^{18} reduces dramatically, and the hydrophobic core observed at acidic pH is severely disrupted. We suggest that the disruption of the C-terminal helix renders the E5 analog fusion-inactive at neutral pH. Furthermore, the decrease of the hinge and the reduction of fusion activity in G13L reveal the importance of the hinge in fusion activity. Also, the decrease in the C-terminal helix and the reduction of fusion activity in L17A demonstrates the importance of the C-terminal helix in fusion activity. Based on these biophysical studies, we propose a model that illustrates the structural change of the HA2 fusion peptide analog and explains how the analog interacts with the lipid bilayer at different pH values.

Membrane fusion plays a vital role in a large and diverse number of essential biological processes. For example, infection by enveloped viruses involves fusion of viral and cellular membranes with subsequent transfer of viral genetic material into the cell. Hemagglutinin (HA)[1] is a homotrimeric surface glycoprotein of the influenza virus with a relative molecular mass of 220 kDa. Each monomer of HA consists of the receptor-binding HA1 domain (328 residues) and the membrane-interacting HA2 domain (221 residues) linked by a single disulfide bond. The membrane fusion activity of HA has been measured both *in vivo* and *in vitro* by a variety of techniques, including hemolysis (1), polykaryon formation (2), resonance energy transfer (3), liposome cell fusion (4), spin-labeled electron paramagnetic resonance (5), electron microscopy (6), flow cytometry (7), electron spin resonance, and Fourier transform infrared (8). The N-terminal 20 residues of the HA2 domain have been identified as the fusion peptide, which is capable of inserting into the target membrane and thereby plays a crucial role in triggering membrane fusion. The crystal structure of soluble trimers (BHA) at neutral pH, in which each HA2 chain after residue 175 is cleaved, revealed that the fusion peptide is buried inside the protein (9). In the crystal structure study, $TBHA_2$ was prepared by successive digestion with trypsin and thermolysin from BHA at pH 5.0. Each monomer of $TBHA_2$ consists of residues 38–175 of the HA2 chain and residues 1–27 of the HA1 chain linked by a disulfide bridge, and the fusion peptide becomes exposed to the aqueous phase in the crystal structure of $TBHA_2$ (10). The difference in the location of the fusion peptide between BHA and $TBHA_2$ accounts for the membrane fusion induction between viral and endosomal membranes occurring at acidic pH for HA.

A comparison of the fusion peptide sequences (20 amino acids) in various subtypes of influenza virus A strains (11, 12) demonstrated that residues Gly^{1}–Glu^{11}, Gly^{13}, Trp^{14}, and Gly^{16} are conserved. Also, Gly^{20} is rather conserved with only one exception of Val^{20} in the A/duck/Hong Kong/231/77 virus strain. Position 12 includes either Gly or Asn, position 17 includes either Met or Leu, and position 18 includes either Ile or Val. Thus, the native fusion peptide of the influenza HA2 is highly hydrophobic, extremely aggregative, and hardly soluble in aqueous solution. The fusion activities of several HA2 fusion peptide mutants have been extensively studied. For example, the fusion peptide without its C-terminal residues 17–20 was fusogenicity inactive (13). Replacement of Glu^{11} with Pro^{11} resulted in a marked decrease in α helical content, concomitant with an almost complete loss of fusogenicity (14). Replacing the

* This work was supported by National Science Council Grants NSC-89-2113-M-001-015 (to C. C.) and NSC-90-2320-B-001-047 and NSC-89-2316-B-001-018 (to S. H. W.) and by funds from Academia Sinica. The costs of publication of this article were defrayed in part by the payment of page charges. This article must therefore be hereby marked "*advertisement*" in accordance with 18 U.S.C. Section 1734 solely to indicate this fact.

‖ To whom correspondence may be addressed: Inst. of Biological Chemistry, Academia Sinica, Taipei 115, Taiwan. Tel.: 886-2-2785-5696, Ext. 7101; Fax: 886-2-2653-9142; E-mail: shwu@gate.sinica.edu.tw.

‡‡ To whom correspondence may be addressed: Inst. of Biomedical Sciences, Academia Sinica, Taipei 115, Taiwan. Tel.: 886-2-2652-3035; Fax: 886-2-2788-7641; E-mail: bmchinp@ccvax.sinica.edu.tw.

[1] The abbreviations used are: HA, hemagglutinin; BHA, bromelain-solubilized hemagglutinin ectodomain; $TBHA_2$, a proteolytic fragment of the low-pH form of BHA; DPC, dodecylphosphocholine; NOE, nuclear Overhauser enhancement; NOESY, NOE spectroscopy.

TABLE I
Amino acid sequences of native fusion peptide and its analogs of influenza hemagglutinin HA2

Peptide	Amino acid sequence	Remarks
Native	GLFGAIAGFIEGGWTGMIDG	
E5	GLF**E**AIA**E**FIEGGW**E**G**L**I**E**G	Gly^4, Gly^8, Thr^{15}, Asp^{19} → Glu; Met^{17} → Leu
G13L	GLFEAIAEFIEG**L**WEGLIEG	Gly^{13} → Leu in E5 peptide
L17A	GLFEAIAEFIEGGWEG**A**IEG	Leu^{17} → Ala in E5 peptide

N-terminal Gly^1 with Glu^1 eliminated viral fusion activity (15), but the fusion activity stayed the same with a Gly^1 → Ala^1 substitution (16). Mutational studies of the fusion activity for the two Ala residues in the N terminus showed that Ala^5 tolerated a smaller (Gly) hydrophobic side chain and that Ala^7 tolerated a larger (Val) hydrophobic side chain (17). A negatively charged E5 analog was found to possess fusion activity at acidic pH (14, 18), similar to that of the native fusion peptide. In addition to triggering fusion activity, the E5 analog has also been found to promote antisense the entrance of oligonucleotides into the cytosol of mammalian cells upon permeabilization of the plasma membrane (19). The specific angle of insertion of the peptide into the membrane plane was observed to be an important characteristic for the fusion process for both intact and synthetic fusion peptides (8, 20).

To date, structural studies of the membrane-bound state of the HA2 fusion peptide and of its analogs have been performed using several biophysical techniques. Upon binding to synthetic liposomes or lipids, the native fusion peptide and its analogs possess higher α-helical contents (18, 21). The NMR solution structures of the native fusion peptide with a host-guest system of influenza hemagglutinin (22) and of the E5 peptide in dodecylphosphocholine (DPC) micelles (23) have been determined. In the present study, we applied fluorescence, CD, and NMR methods to carry out biophysical studies in SDS micelles for the E5 analog and its two point mutants, G13L and L17A (Table I), both of which possess much less fusion activity than the E5 analog (12). We then developed a model that describes the structural change of the fusion peptide analog and how the analog interacts with the lipid bilayer at different pH values, on the basis of the determined three-dimensional structures and results from CD and fluorescence experiments. Comparison of our model with the two recently reported models (22, 23) is then discussed.

EXPERIMENTAL PROCEDURES

Sample Preparation—Three fusion peptide analogs of HA2 of virus strain A/PR/8/34 (8), E5 and its two point mutants, G13L and L17A, were synthesized in automated mode by a solid phase synthesizer (model 431 A; Applied Biosystems, Foster City, CA). These synthetic peptides were cleaved from the resins with trifluoroacetic acid and purified by reverse-phase high pressure liquid chromatography. The sequences of these peptides were ascertained by electrospray mass spectrometry and by amino acid analysis. Deuterated SDS was purchased from Cambridge Isotope (Woburn, MA). Unless otherwise specified, all of the reagents and solvents were obtained commercially of reagent grade and used without further purification.

CD Experiments—CD experiments were collected using an AVIV CD 202 spectrometer (AVIV, Lakewood, NJ) calibrated with (+)-10-camphorsulfonic acid at 25 °C. In general, a 2-mm path-length cuvette with 50 μM (or 20 μM) fusion peptide analog in 20 mM phosphate was used for CD experiments. The CD spectra of each analog at a molar ratio of 1:100 (peptide/SDS) at different pH values (pH 3.5–9.0) were recorded. Each of the CD data was obtained from an average of three scans with 1-nm bandwidth. The spectra were recorded from 180 to 260 nm at a scanning rate of 38 nm/min with a wavelength step of 0.5 nm and a time constant of 100 ms. After background subtraction and smoothing, all of the CD data were converted from CD signal (millidegree) into mean residue ellipticity (deg cm^2 $dmol^{-1}$). The secondary structure content of each peptide was estimated from the CD spectra according to the method of Sreerama and Woody (24).

Fluorescence Measurements—Penetration of fusion peptides into membranes can be determined by monitoring changes in intrinsic fluorescence of aromatic amino-acids (Trp, Tyr, or Phe) contained in the peptide sequence. All of the fluorescence experiments were performed on a Hitachi F-4010 fluorescence spectrofluorometer at ambient temperature. An excitation wavelength of 280 nm was used to record spectra from 290 to 490 nm with a data interval of 1 nm. The response time was set at 2 s with a scan rate of 60 nm·min^{-1}. Excitation and emission slits of 5 and 1.5 nm, respectively, were used for measurements in the presence and absence of SDS micelles. Acrylamide was used for tryptophan fluorescence quenching experiments. An incremental amount of acrylamide stock solution (1 M) was added to the peptide (10 μM) solutions to make final concentrations of acrylamide up to 50 mM in the presence of SDS micelles at pH 4.3 and 7.3. The data were analyzed according to the following Stern-Volmer equation (25).

$$F_0/F = 1 + K_{SV}[Q] \quad \text{(Eq. 1)}$$

Where F_0 and F are the fluorescence intensities in the absence and the presence of quencher [Q], respectively. K_{SV}, calculated as the slope of the Stern-Volmer plot, is the Stern-Volmer quenching constant and is a measure for the accessibility of the tryptophan to acrylamide.

NMR Experiments—NMR measurements were carried out on a Bruker AMX-500 or an AVANCE-600 spectrometer. The samples for the NMR experiments contained about 0.35 ml of 2 mM peptide in SDS micelles (peptide/SDS 1:100) using 20 mM phosphate buffer to adjust pH values (pH 4.0–9.0). pH values were measured with a dissolved oxygen microelectronic pH vision model PHB-9901 pH meter equipped with a 4-mm electrode. All of the reported pH values were direct readings from the pH meter without correction for the isotope effect. To monitor the exchange rates of labile protons, the concentrated sample in H_2O was lyophilized only once and redissolved in D_2O (99.99% D). The NMR spectra were acquired immediately and thereafter at appropriate time intervals. All of the chemical shifts were externally referenced to the methyl resonance of 2,2-dimethyl-2-silapentane-5-sulfonate (0 ppm). Double quantum filtered scalar-correlated spectroscopy (26), total correlation spectroscopy (27), and NOESY (28) were collected with 512 t_1 increments with 2K complex data points. All spectra were recorded in time-proportioned phase increment mode (29). The titration experiments of the chemical shift *versus* pH were carried out using one- and two-dimensional NMR experiments at 310 K for E5 and G13L. The titration experiment was not performed for L17A, because of its severe precipitation at neutral pH. Low temperature studies employed a temperature-controlled stream of cooled air using a Bruker BCU refrigeration unit and a B-VT 2000 control unit. Water suppression was achieved by 1.4 s of presaturation at the water frequency or by the gradient method (30). All spectra were collected with 6024.1- and 7788.16-Hz spectral widths for AMX-500 and AVANCE-600, respectively.

The data were transferred to an SGI O_2 work station (200 MHz R5000SC; Silicon Graphics, CA) for the processing and further analysis using Bruker XWINNMR and AURELIA software packages (Karlsruhe, Germany). All data sets acquired were zero-filled to equal points in both dimensions prior to further processing. A 60°-shifted skewed sine bell window function was applied in all NOESY and total correlation spectroscopy spectra, and a 20°- or 30°-shifted skewed sine bell function was used for all correlated spectroscopy spectra. To help resolve spectral overlap, the data were collected at different temperatures.

Structure Calculations—Distance restraints of fusion peptide analogs were derived primarily from the 200-ms NOESY spectrum recorded in SDS micelles at 310 K, pH 4.0. Comparison was made to the 100-ms NOESY spectrum to assess possible contributions from spin diffusion. Peak intensities were classified as large, medium, small, and very small, corresponding to the upper bound interproton distance restraints of 2.5, 3.5, 4.5, and 6.0 Å, respectively. An additional correction of 1.0 Å was added for methylene and methyl groups. Backbone dihedral restraints were inferred from $^3J_{NH}$ coupling constants, with ϕ restrained to $-120 \pm 30°$ for $^3J_{NH\alpha} > 8$Hz and $-60 \pm 30°$ on $^3J_{NH\alpha} < 6$Hz. Three-dimensional structures were generated using a simulated annealing and energy minimization protocol in the program X-PLOR 98

(31). Hydrogen bond restraints were included only in the final stage of refinement, and all of the peptide bonds were defined as *trans*. Average structures were calculated using the final set of refined structures and were further energy minimized to ensure correct local geometry. The INSIGHT II (Molecular Simulation Inc., San Diego, CA), MOLMOL (32), and GRASP (33) software programs were used to visualize sets of structures and to calculate and draw the electrostatic surface potential of the final three-dimensional models. The convergence of the calculated structures was evaluated in terms of the structural parameters, that is, the root mean square deviation from the experimental distance and dihedral constraints, the values of the energy statistics (F_{noe}, F_{tor}, and F_{repel}), and the root mean square deviation from the idealized geometry. The distributions of the backbone dihedral angles of the final converged structures were evaluated by the representation of the Ramachandran dihedral pattern, indicating the deviations from the sterically allowed (ϕ and ψ) angle limits using PROCHECK-NMR (34).

RESULTS

Conformational Changes at Different pH Values—CD spectroscopy was used to determine whether the peptides undergo a conformational change upon interaction with lipid micelles at different pH values. The CD spectra of three analogs at various pH values in SDS micelles all showed that the conformations of the analogs are pH-dependent (Fig. 1). The observations of 208- and 222-nm negative ellipticities and of isodichroic point at 203, 203, and 204 nm for E5, G13L, and L17A, respectively, revealed that a random coil and an α-helix are in equilibrium in these analogs. Based on the standard values of the mean residue molar ellipticity at 222 nm, 4000 deg cm^2 dmol^{-1} for the random coil and -38000 deg cm^2 dmol^{-1} for the α-helix (35), we estimated the following α-helical content for each analog at pH 7.0 and 3.5, respectively: 48 and 72% for G13L; 43 and 62% for E5; and 24 and 43% for L17A. Clearly, G13L exhibits the highest content of α-helical structures, whereas L17A contains fewest α-helical structures at both neutral and fusogenic pH. At pH $>$ 6.0, the negative ellipticity shifted to the value of $\sim$200 nm in L17A, indicating that L17A is mostly unstructured under this condition. Interestingly, the helical content of L17A at acidic pH is nearly the same as that of E5 at neutral pH.

Depth of Tryptophan Penetration to Membrane—All three analogs contain a Trp residue at position 14. To verify the interaction of the fusion peptide analogs and the SDS micelles, the steady-state fluorescence emission spectra of these three analogs were measured. It is suggested that the observation of a blue shift upon interaction of the peptides with the negatively charged vesicles indicates that the tryptophan moiety has penetrated into the vesicle bilayer. As shown in Fig. 2*A*, the E5 peptide at neutral pH without SDS micelles exhibited a emission maximum at 352 nm and reached a maximum of 336 nm in the presence of SDS micelles. This observation of a blue shift verifies the transfer of tryptophan to a more hydrophobic environment and verifies that there is an interaction between the E5 analog and micelles. At acidic pH, a further blue shift was observed, indicating a deeper insertion of tryptophan into lipid bilayers. Interestingly, G13L possesses characteristics in its fluorescence data very similar to those of the E5 peptide (Fig. 2*B*). The fluorescence spectra of L17A shown in Fig. 2*C*, however, revealed a different characteristic. The emission maximum of L17A remained at $\sim$352 nm in aqueous solution with or without micelles at neutral pH, revealing that at neutral pH it hardly interacts with micelles. At acidic pH the emission maximum shifted to 336 nm, the same as the maximum of E5 at neutral pH. The result of fluorescence emission experiments seems to indicate that the structure of E5 at neutral pH is quite similar to that of L17A at acidic pH. To further verify that tryptophan inserts deeper into lipid bilayers at acidic pH, we carried out acrylamide fluorescence quenching experiments. Fig. 3*A* shows the Stern-Volmer plot for E5, G13L, and L17A peptides in SDS micelles at pH 4.3 and 7.3. A comparison of the

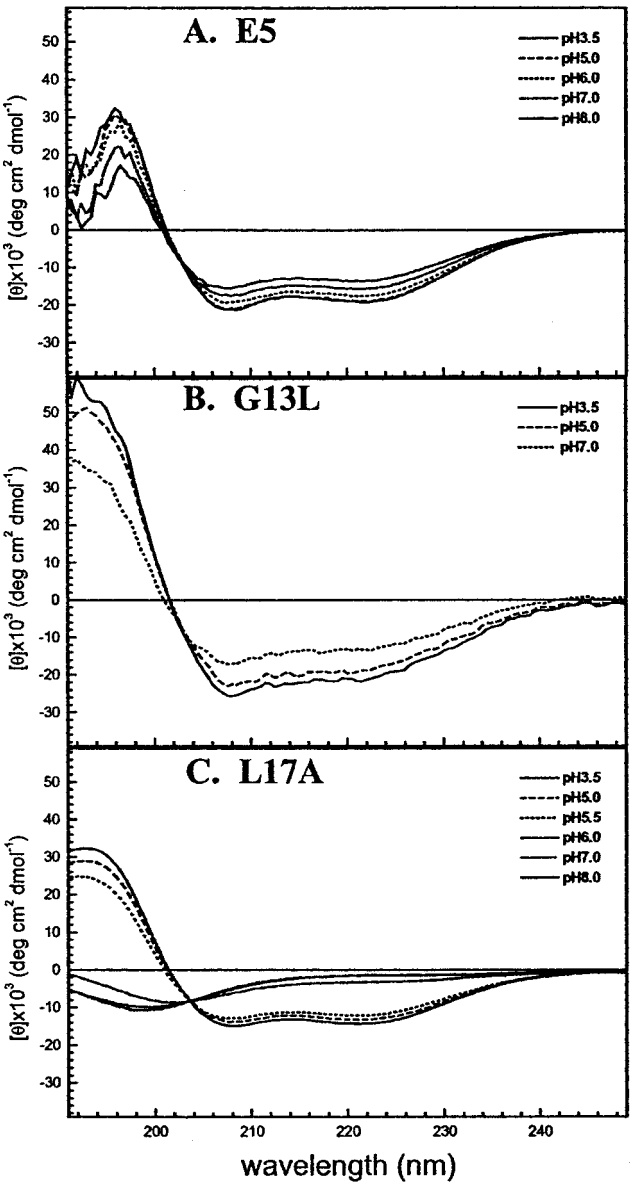

FIG. 1. **CD spectra of E5 (*A*), G13L (*B*), and L17A (*C*) analogs at different pH values in SDS micelles with a molar ratio of peptide/SDS of 1:100 at 25 °C are shown.** The isodichroic point at 203, 203, and 204 nm for E5, G13L, and L17A, respectively, was observed, indicating that an α-helix and a random coil are in equilibrium in these analogs.

Stern-Volmer quenching constants (M^{-1}) among these peptides is shown in Fig. 3*B*. The three analogs at acidic pH all possess a smaller K_{SV} value compared with that at neutral pH, indicating that the Trp residue inserts deeper into lipid bilayers at acidic pH. In addition, the K_{SV} value of E5 peptide at neutral pH is nearly identical to that of L17A at acidic pH, in good agreement with the finding that the emission maximum of E5 at neutral pH is the same as that of L17A at acidic pH.

Resonance Assignments and Secondary Structure Determination—With well dispersed NMR data, resonance assignments for E5, G13L, and L17A were accomplished using standard procedures. The total correlation spectroscopy and double quantum filtered scalar-correlated spectroscopy spectra were used to assign the spin systems, and the NOESY spectra were used to make sequential connections between spin systems. In addition, the NMR experiments obtained at different temperatures (285, 295, and 310 K) at both neutral and fusogenic pH values were used to assign the overlapping peaks. Fig. 4 shows

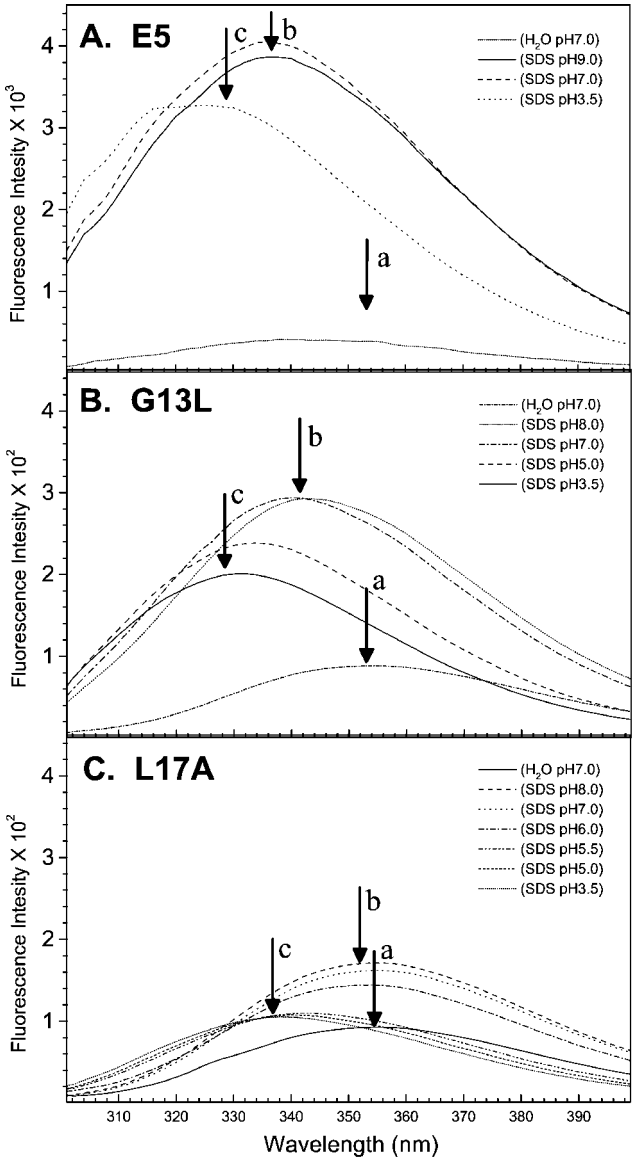

FIG. 2. **Fluorescence emission spectra of E5 (*A*), G13L (*B*), and L17A (*C*) acquired in the absence and presence of SDS micelles at different pH values.** For clarity, the emission maximum at three different conditions for each analog is indicated by a *labeled arrow*. *Arrow a*, in the aqueous solution at pH 7.0; *arrow b*, in the presence of SDS micelles at pH 7.0; *arrow c*, in the presence of SDS micelles at pH 3.5.

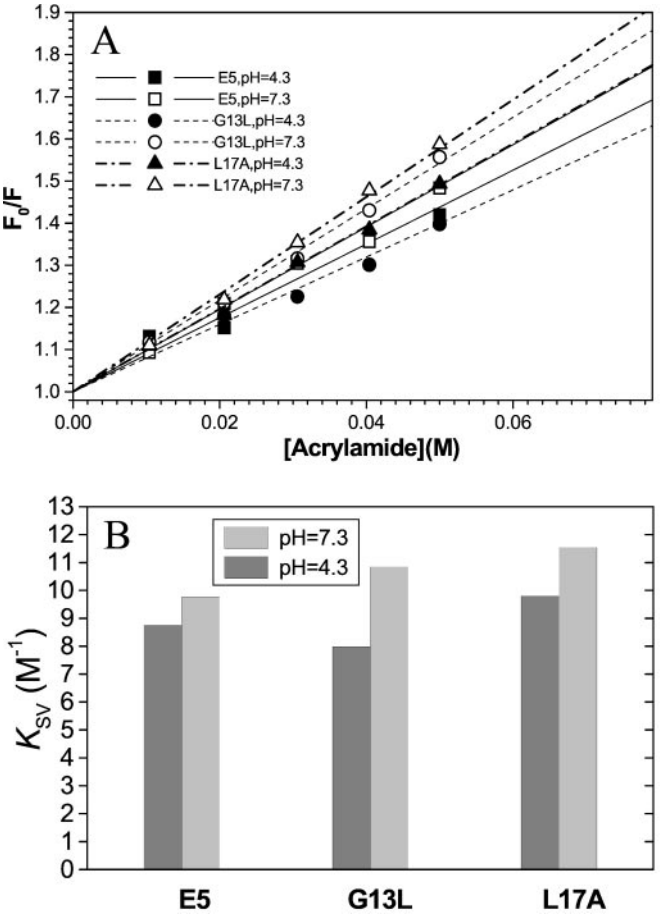

FIG. 3. **Trp fluorescence quenching experiments of HA2 fusion peptide analogs by acrylamide in the presence of SDS micelles are shown.** *A*, Stern-Volmer plots for E5, G13L, and L17A peptides in SDS micelles at pH 4.3 and 7.3. The peptide concentration is 10 μM and acrylamide concentration is given on the *x* axis. *B*, a comparison of the Stern-Volmer quenching constants (M^{-1}) for E5, G13L, and L17A in the presence of SDS micelles at pH 4.3 and 7.3.

the representative regions of the NOESY spectra involving the backbone protons for E5, G13L, and L17A at pH 4.0, respectively. In general, the observations of weaker $d_{\alpha N}(i, i+1)$ and stronger $d_{\alpha N}(i, i)$ and $d_{NN}(i, i+1)$ connectivities, together with $d_{\alpha N}(i, i+3)$, $d_{\alpha N}(i, i+4)$, and $d_{\alpha\beta}(i, i+3)$ NOEs, suggest a stabilization of the α-helical structure. We observed a set of α-helical NOEs in the N-terminal segment of Ile^2–Glu^{11} for all three analogs at acidic pH. In the C-terminal region, the absence of $d_{\alpha N}$ (10, 13) NOE and the observation of a nonhelical medium range NOE of $d_{\alpha\alpha}$ (9, 13) indicated the lack of an α-helix in the E5 analog in the Gly^{12}-Gly^{13} dipeptide. In the Trp^{14}–Ile^{18} segment of E5, the weaker intensities of $d_{\alpha\beta}$ (14, 17), $d_{\alpha\beta}$ (15, 18), $d_{\alpha N}$ (14, 17), and $d_{\alpha N}$ (15, 18) NOEs indicate that this region possesses some α-helical structures but that it is less populated than the N-terminal α-helix. Compared with the C-terminal structure of the E5 peptide, structural differences were seen in the C-terminal regions in G13L and L17A, both of which possess much less fusion activity than E5. In G13L, neither $d_{\alpha\alpha}$ (9, 13) nor $d_{\alpha N}$ (9, 13) NOEs were found, and two intensive α-helical NOEs, $d_{\alpha N}$ (10, 13) and $d_{\alpha N}$ (13, 16), were identified instead, indicating that a replacement of Gly^{13} with Leu^{13} (G13L) increased the α-helical conformation in residues 12–13. Further, based on the presence of stronger α-helical NOEs in the C terminus than those present in the C terminus of E5, we concluded that G13L possesses higher C-terminal α-helical contents than the E5 peptide. Therefore, the G13L analog likely forms an extended helix. In contrast, the NMR data of L17A at acidic pH show that its C-terminal α-helix almost disappears with very small $d_{\alpha N}$ (14, 17), $d_{\alpha\beta}$ (14, 17), and $d_{\alpha\beta}$ (15, 18) NOEs and the disappearance of the $d_{\alpha N}$ (15, 18) α-helical NOE in Trp^{14}–Ile^{18}. A comparison of NOEs between E5 and L17A, however, does not show any significant change in the N-terminal α-helix and the hinge region. Consequently, the main structural difference between E5 and L17A comes from the C-terminal α-helix in the Trp^{14}–Ile^{18} segment. Fig. 5 shows a comparison of the $C^{\alpha}H$ chemical shift between E5 and G13L and between E5 and L17A, respectively. The substitution of Leu for Gly^{13} (G13L) lowers the $C^{\alpha}H$ chemical shifts in its neighboring residues (Ile^{10}–Gly^{12} and Trp^{14}), revealing that the segment of Ile^{10}–Trp^{14} in G13L contains a higher propensity to form a helical structure. The substitution of Ala for Leu^{17} (L17A), however, increases the $C^{\alpha}H$ chemical shift at residues Trp^{14} and Glu^{15}, indicating a reduction in the C-terminal helix. Thus, the derived secondary structures based on NOE connectivities and $C^{\alpha}H$ chemical shifts are in good

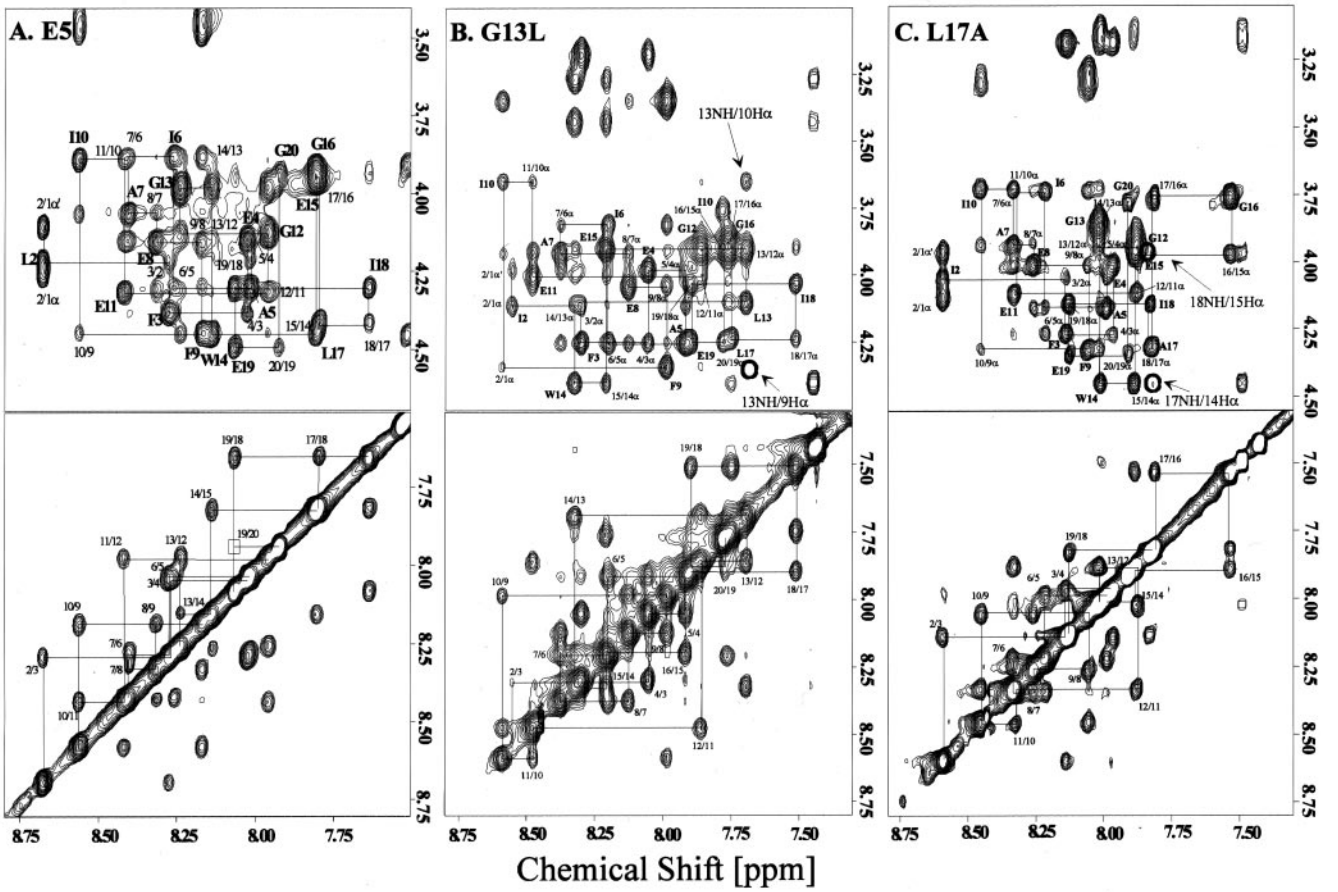

FIG. 4. **The fingerprint and HN/HN regions of NOESY spectra of E5 (*A*), G13L (*B*), and L17A (*C*) in SDS micelles at pH 4.0 and 310 K.** The sequential connectivities are annotated, and the intraresidue NOEs in the fingerprint region are indicated with a one-letter amino acid code and a residue number. The observation of $d_{\alpha N}$ (10, 13) NOE and the disappearance of $d_{\alpha N}$ (9, 13) in G13L are specifically indicated by *arrows*. The two α-helical NOEs, $d_{\alpha N}$ (14, 17) and $d_{\alpha N}$ (15, 18) in L17A, which were hardly seen, were also indicated by *arrows*.

agreement. At neutral pH, the N-terminal α-helix remains and the C-terminal α-helix of E5 is dramatically reduced, as deduced by the disappearance or significantly less intensity of medium α-helical NOEs: $d_{\alpha\beta}$ (14, 17), $d_{\alpha\beta}$ (15, 18), $d_{\alpha N}$ (14, 17), and $d_{\alpha N}$ (15, 18). Therefore, the pH-induced structural change of the E5 peptide at different pH values is mainly due to the C-terminal α-helix. To check the rigidity of the structure and to identify the hydrogen bonds, we measured the amide-proton exchange rates for these analogs in SDS micelles using one- and two-dimensional NMR for E5, G13L, and L17A at acidic pH. The N-terminal amide protons (Ala^5–Ile^{10}) were still present in all three analogs after dissolution in D_2O for more than 30 min, suggesting that these residues are likely to form strong hydrogen bonds. Thus, the exchange rates show that the N-terminal α-helix in these three analogs is more stable and rigid than the C-terminal one. The $^3J_{NH\alpha}$ coupling constants estimated from the two-dimensional double quantum filtered scalar-correlated spectroscopy spectra imply that N-terminal residues Leu^2–Glu^{11} possess smaller coupling constants (< 6Hz), which is in agreement with the formation of an α-helix in this region. Fig. 6 provides an NMR summary for these three analogs, respectively. All of the NMR parameters support that E5 forms a stable α-helical structure in Leu^2–Glu^{11} and a loose α-helix in the C terminus at Trp^{14}–Ile^{18}, with Gly^{12}-Gly^{13} forming a hinge. G13L extends the N-terminal helix to the C-terminal region, and L17A nearly loses the C-terminal short helix entirely.

Analysis of pH Titration Experiments—On the basis of the titration curves of the chemical shift *versus* pH, we determined the pK_a values of five Glu residues in the sequence (Glu^4, Glu^8, Glu^{11}, Glu^{15}, and Glu^{19}) of E5 and G13L peptides in SDS micelles. We found that they are nearly identical to the values in DPC micelles reported by Dubovskii *et al.* (23). In addition, the chemical shift change for the $C^{\alpha}H$ of Ile^{10} and Glu^{15} of E5 peptide in these two micellar solutions at different pH values are also very similar. However, in G13L, we only observed very small chemical shift changes of Glu^{15} $C^{\alpha}H$ and did not detect any shift change of Ile^{10} $C^{\alpha}H$ at different pH values. Evidently, the backbone structure at Ile^{10} and its nearby region of G13L is very rigid and pH-independent.

Tertiary Structures—Because E5 possesses membrane-penetrating activity similar to the native fusion domain (36), we first determined the E5 structure in SDS micelles at fusogenic pH. A set of 372 restraints was used for simulated annealing and energy minimization calculations using the software program X-PLOR. Among these restraints, 356 are interproton distance restraints, 10 are hydrogen bond restraints, and 6 are dihedral-angle restraints. Each structure was checked according to geometric deviation, total energy, and distance violation. Thirteen structures were chosen to represent the ensemble of NMR structures on the basis of the lowest target function and minimal distance and torsional angle restraint violations in the final stage. All of these structures were consistent with both experimental data and standard covalent geometry and displayed no violations greater than 0.5 Å for distance restraints. The NMR solution structures demonstrate that the E5 peptide is composed of two helical segments; one section is located in the N terminus (residues Leu^2–Glu^{11}), and the other is located in the C-terminal region (Trp^{14}–Ile^{18}). In the C-terminal Trp^{14}–Ile^{18} segment, the backbone ϕ and ψ dihedral angles are

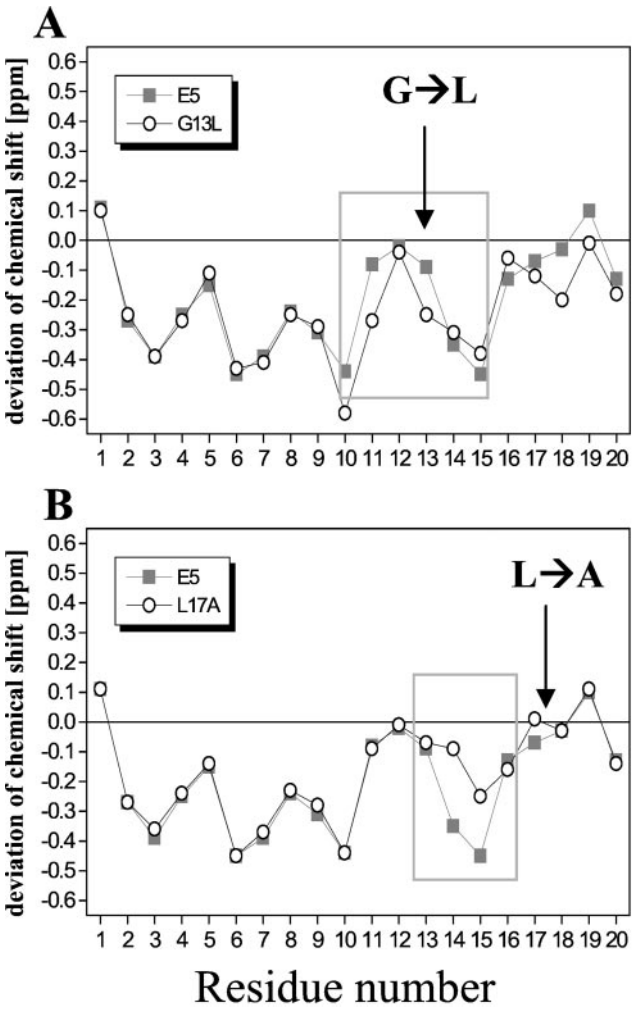

FIG. 5. **Comparisons of the C$^{\alpha}$H chemical shift of G13L and E5 (*A*) and L17A and E5 (*B*) are shown.** The substitution of Leu for Gly^{13} (G13L) lowers the C$^{\alpha}$H chemical shift in its neighboring residues (Ile^{10}–Gly^{12} and Trp^{14}), revealing that this segment contains a higher propensity to form a helical structure. However, the substitution of Ala for Leu^{17} (L17A) increases the C$^{\alpha}$H chemical shift at residues Trp^{14} and Glu^{15}, indicating a reduction of the C-terminal α-helix.

close to the values for 3_{10}-helix ($\phi = -60°$ and $\psi = -30°$) and two (i, i+3) hydrogen bonds, Trp^{14} CO/Leu^{17} NH and Glu^{15} CO/Ile^{18} NH, were observed; thus it is confirmed that Trp^{14}–Ile^{18} forms a 3_{10}-helix. Gly is known to be a helix-breaking residue. As expected, Gly^{12}-Gly^{13} terminates the N-terminal α-helical structure and forms a hinge structure. For clarification, superimpositions of backbone heavy atoms (N, Cα, and C′) from residues 2–18, 2–11, and 14–18 with root mean square deviations of 1.26, 0.44, and 0.29 Å, respectively, were calculated and are shown in Fig. 7. The precise orientation of the two helical segments could not be determined because of the lack of medium and long range NOEs between the two helices. An angle between the two helical axes of ~120° was consistently observed in the ribbon representation of structure. The structural statistics on the final set of structures are given in Table II. Interestingly, because of the twist of the central hinge in E5, the charge distribution of E5 forms an amphipathic bent helical structure with five negatively charged Glu residues located on one side and with the hydrophobic residues located on the opposite side (Fig. 8). Using the same protocol, we also generated the solution structures of G13L and L17A at acidic pH. A comparison of the ribbon diagrams of the three analogs is shown in Fig. 9.

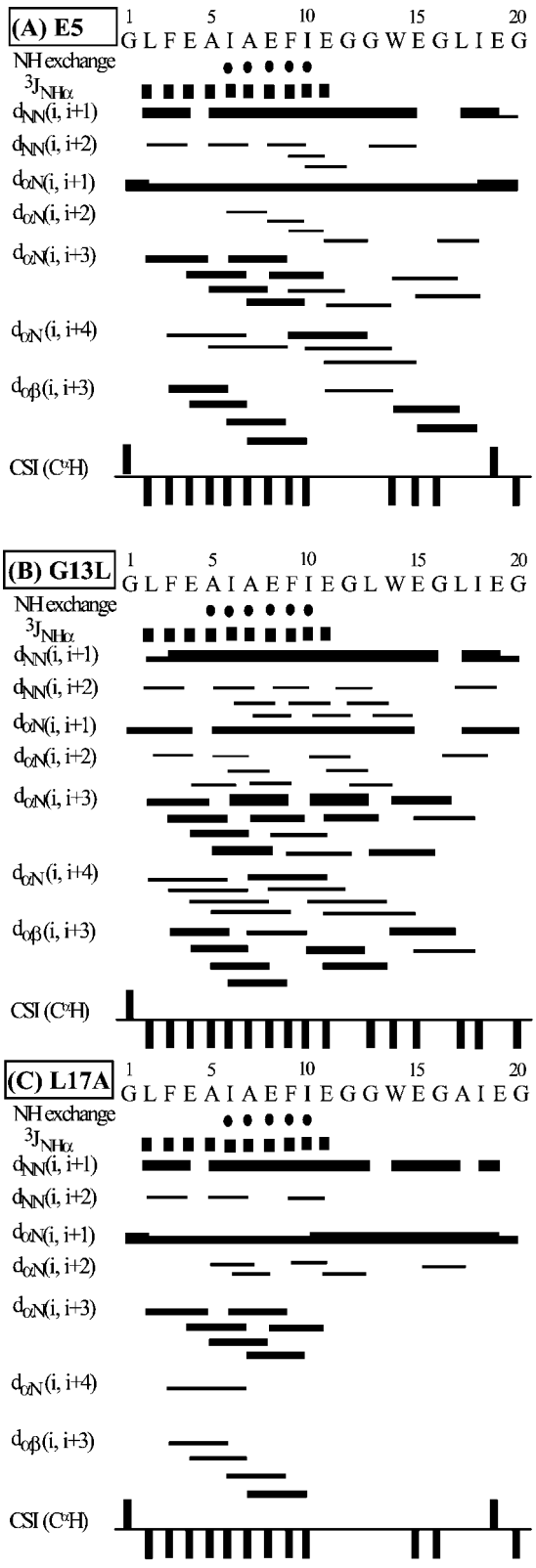

FIG. 6. **Summaries of the amide proton exchange rates, the $^3J_{NH\alpha}$ coupling constants, NOE connectivities, and C$^{\alpha}$H chemical shift index for E5, G13L, and L17A at pH 4.0 are shown.** Slow and medium exchanging amide protons are represented by *filled* and *open circles*, respectively. The $^3J_{NH\alpha}$ coupling constants smaller than 6 Hz are indicated by *filled squares*. *Bar thickness* indicates the intensity of NOE connectivity, with *thicker bars* representing stronger NOEs. *Negative bars* in the chemical shift index indicate upfield shifts of more than 0.1 ppm of the C$^{\alpha}$H compared with the expected random coil C$^{\alpha}$H chemical shift. *Positive bars* indicate downfield shifts of more than 0.1 ppm of the C$^{\alpha}$H compared with the expected random coil C$^{\alpha}$H value.

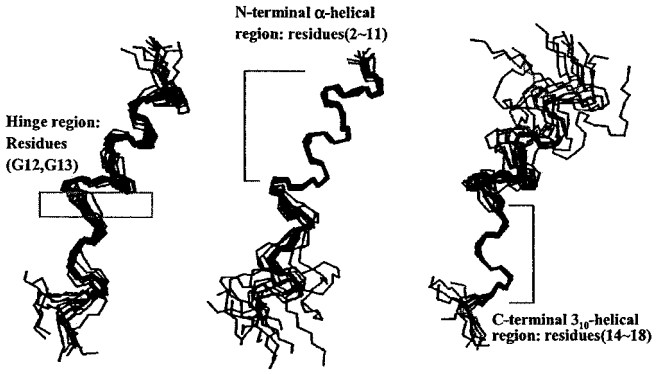

FIG. 7. **Superposition of the backbone (N, C$^{\alpha}$, and C′) atoms of 13 NMR structures of the E5 analog obtained from simulated annealing and energy minimization calculations.** The structures are best fitted to residues 2–18 (*A*), 2–11 (*B*), and 14–18 (*C*), respectively.

TABLE II
Structural statistics on the final set of simulated annealing structures of E5 in SDS micelles

Restraints used	
Distance restraints	
Intraresidue	172
Sequential	140
Medium and long range	44
Total distance restraints	356
Hydrogen bonds	10
Dihedral angles	6
Statistics for the final X-PLOR structures	
Number of structures in the final set	13
X-PLOR energy (kcal · mol^{-1})	
E_{NOE}	12.73 ± 1.43
E_{cdih}	1.83 ± 0.68
$E_{bond} + E_{angle} + E_{improper}$	591.55 ± 5.32
E_{elec}	2.25 ± 0.26
NOE violations	
Number > 0.5 Å	None
Root mean square deviation (Å)	0.05
Deviation from idealized covalent geometry	
Angle (deg)	2.58 ± 0.46
Improper (deg)	3.99 ± 0.03
Bonds (Å)	0.01
Root mean square deviation (Å)	
Backbone (N, C$^{\alpha}$, C′)	
Residues (2–18)	1.26 ± 0.32
Residues (2–11)	0.44 ± 0.12
Residues (14–18)	0.29 ± 0.09
Ramachandran data	
Residues in most favored regions (%)	85.2
Residues in allowed regions (%)	12.8
Residues in generously allowed regions (%)	0.5
Residues in disallowed regions (%)	1.5

DISCUSSION

We performed CD, fluorescence, and NMR experiments to investigate the structural changes of three fusion peptide analogs of influenza virus HA2 in SDS micelles at different pH values. As described above, E5 possesses fusion activity similar to the native fusion peptide, whereas G13L and L17A exhibit much less fusion activity than the E5 analog. CD experiments revealed that G13L possesses higher α-helical content than E5 at acidic and neutral pH, indicating that α-helical structure alone cannot cause fusion activity for influenza HA2 fusion peptide. Both E5 and G13L showed a blue shift in their fluorescence spectra in the presence and absence of SDS micelles at neutral pH, revealing that both analogs penetrate into the micelles and associate with the hydrophobic core in the lipid bilayer at neutral pH. In contrast, the emission maximum of fluorescence spectra of L17A at pH 7.0 remained the same with or without SDS micelles, indicating that SDS micelles are unable to induce any conformational change in L17A at neutral pH. This observation is consistent with our CD data, which show that at neutral pH L17A is mostly unstructured in the presence of SDS micelles and in the aqueous solution. From neutral to acidic SDS micelles, a further blue shift was detected in E5 and G13L, indicating a deeper insertion of both analogs into lipid bilayers. Also, a blue shift of 16 nm (shift from 352 nm to 336 nm) observed in L17A suggested that L17A can penetrate into and interact with the micelles at acidic pH. It is noteworthy that the emission maximum of L17A at acidic pH is the same as that of E5 at neutral pH. Therefore, the characteristic of E5 of peptide insertion into lipid bilayers at neutral pH should be similar to that of L17A at acidic pH. Acrylamide quenching experiments showed that the K_{SV} values for E5, G13L, and L17A at acidic pH are lower than the K_{SV} values at neutral pH in the presence of SDS micelles, indicating that the tryptophan residue is more protected against quenching by acrylamide at acidic pH. Accordingly, fluorescence emission experiments revealed that E5 as well as G13L exhibit a very similar means for peptide insertion into lipid bilayers, even though they possess different fusion activities. This phenomenon indicates that the insertion of a peptide into lipid bilayers does not guarantee whether the peptide is fusion-active.

The NMR solution structure of the E5 peptide in SDS micelles at pH 4.0 is comprised of a regular α-helix in the N-terminal Ile^{2}–Glu^{11} and a 3$_{10}$-helix in the C-terminal Trp^{14}–Ile^{18}, with Gly^{12}-Gly^{13} forming a hinge. Also, the hydrophobic residues in the N- and C-terminal helices form a hydrophobic cluster. We suggest that the fusion peptide inserts into the lipid bilayers with its hydrophobic surface exposed to the apolar interior of the membrane. At neutral pH, the pH-induced structural change of the E5 analog occurs predominantly in the C-terminal helix. The decrease of the C-terminal helix hence breaks the hydrophobic cluster observed at acidic pH, and the fusion activity becomes inactive. A comparison of the solution structures of E5 and G13L shows that the hinge observed in E5 is dramatically reduced in G13L at acidic pH. The decrease of the hinge along with the reduction of fusion activity in G13L reveals the importance of the hinge in fusion activity. By contrast, we found that the main structural difference between E5 and L17A at acidic pH occurs at the C-terminal helix. Therefore, the decrease of the C-terminal helix together with the reduction of fusion activity in L17A demonstrates the importance of the C-terminal helix in fusion activity. Taken together, the structural features that are essential for fusion activities of the influenza fusion peptide can be summarized as follows: 1) a rigid N-terminal helix for disrupting the membrane, 2) a central hinge for twisting and bending N- and C-terminal helices to form a hydrophobic cluster, and 3) a C-terminal 3$_{10}$-helix to span the membrane, thereby facilitating deeper insertion of the peptide and formation of a central hinge at acidic pH.

Taking these results together, we propose a model (Fig. 10) to describe the structural change of the E5 analog and how E5 interacts with the lipid bilayer at different pH values. At neutral pH, a blue shift was observed for the E5 analog in the presence and absence of SDS micelles, implying that there is an interaction between the Trp residue and the lipid bilayer. We thus suggest that Gly^{1}–Trp^{14} is located inside the membrane, with Trp^{14} near the head group of the lipid bilayer, and that the C-terminal region (Glu^{15}–Gly^{20}) is exposed to the aqueous phase. When lowering the pH, the charged residues, Glu^{11} and Glu^{15}, are neutralized, and the C-terminal helix is increased. Under this condition, Glu^{15}–Ile^{18} also inserts into lipid bilayers, and a hydrophobic core is formed among the hydrophobic residues in the N- and C-terminal helices to facilitate the interaction of the E5 analog with the lipid bilayer. The fusion peptide analog then destabilizes the membrane, with the fusion

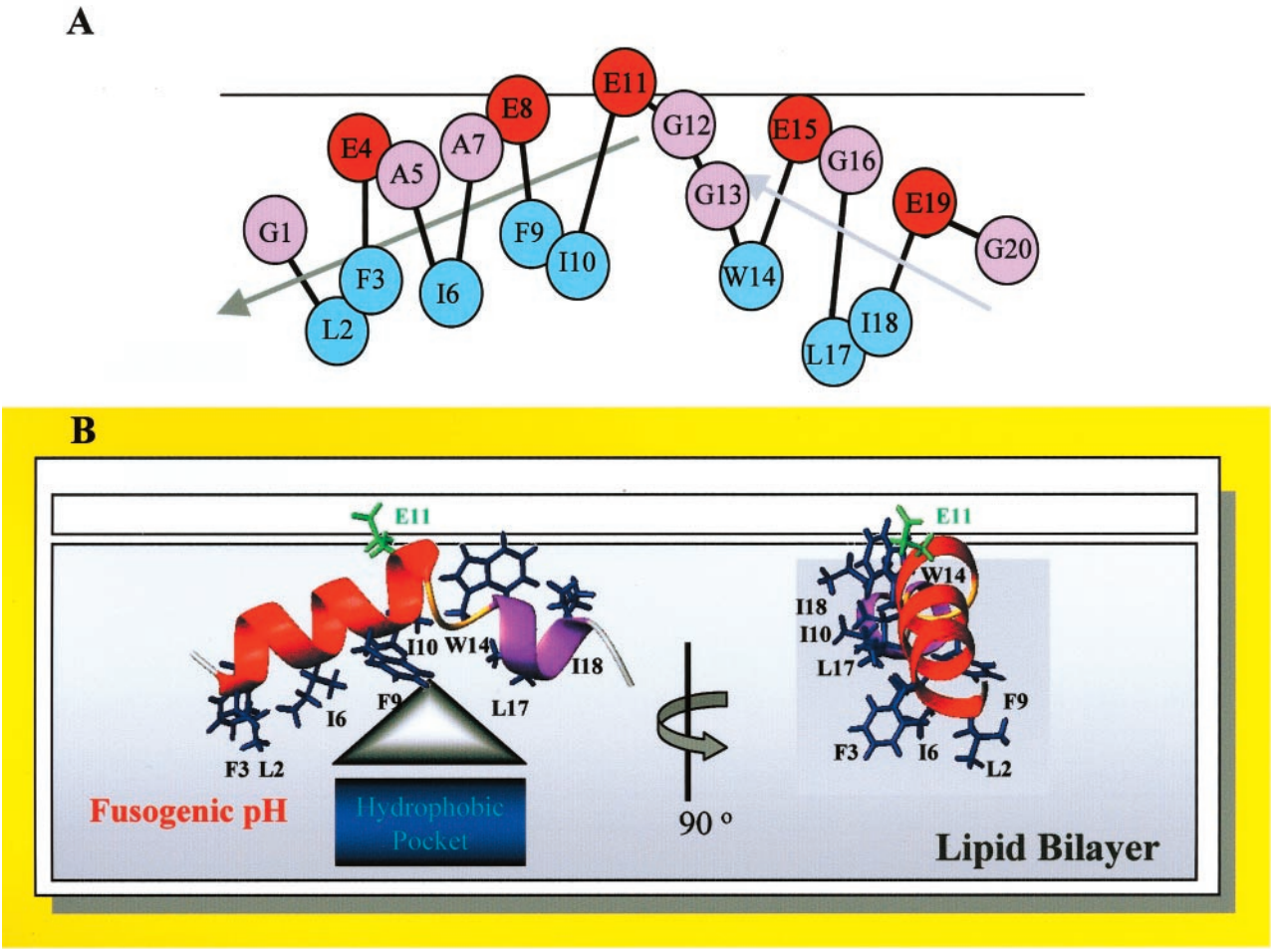

FIG. 8. **The active fusion peptide analog E5 presents a helix-hinge-helix structural motif.** *A*, a cartoon representation of the structure of the E5 analog at fusogenic pH, with a helix-hinge-helix structural motif. *B*, the hinge structure of the E5 analog facilitates the hydrophobic surface of the C-terminal helix to twist to the same side with the hydrophobic surface of the N-terminal α-helix. The helix-hinge-helix structure of E5 forms a hydrophobic pocket consisting of Leu[2], Phe[3], Ile[6], Phe[9], Ile[10], Trp[14], Leu[17], and Ile[18].

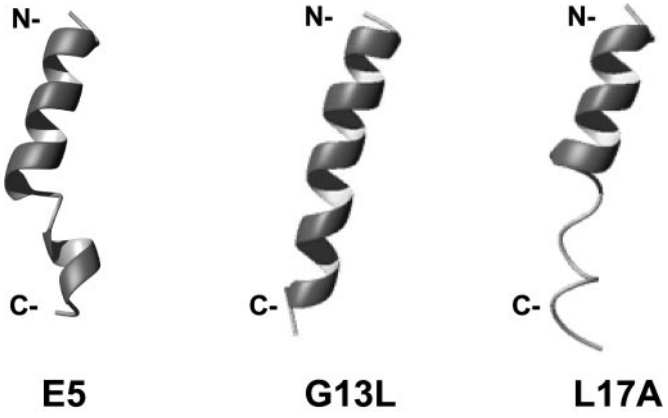

FIG. 9. **A comparison of ribbon diagrams of the three-dimensional structures of E5, G13L, and L17A analogs is shown.** The ribbon structure was produced using the MOLMOL program.

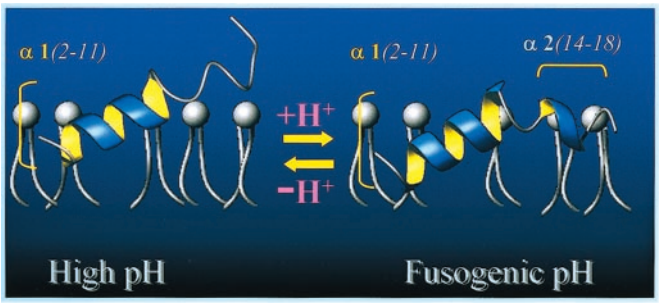

FIG. 10. **A proposed model, based on the results from NMR, CD, and fluorescence experiments, shows the structural change of the E5 analog and how the analog interacts with lipid bilayers at different pH values.** The C terminus is mostly unstructured at high pH and is exposed in the aqueous phase. At fusogenic pH, the helical content in Trp[14]-Ile[18] is increased because of the charge neutralization on Glu[15] and/or Glu[11]. The C-terminal helix then penetrates into the membrane and interacts with the hydrophobic core in the lipid bilayer. In the meantime, the flexible region in Gly[12]-Gly[13] serves to facilitate fusion pore formation. Subsequently, the fusion peptide analog destabilizes the membrane and then triggers membrane fusion.

pore forming with the help of the hinge in the Gly[12]-Gly[13] dipeptide, thereby triggering membrane fusion.

Our proposed model is different from the reported model (23) based on a structural study of the E5 peptide in DPC micelles. The CD spectra showed that the E5 peptide in DPC micelles contains more helical content (50%) at pH 5.4 than at pH 6.7 (40%), which is in good agreement with our finding that the conformation of the E5 peptide in SDS micelles is pH-dependent. The NMR solution structure of the E5 analog in DPC micelles at pH 5.4 and at a detergent-to-peptide ratio of 60 was determined to contain an amphipathic α-helix in residues 2–18, in which 11–18 is flexible. However, the hinge in Gly[12]-Gly[13] dipeptide and pH-induced structural change in the C-terminal helix were not mentioned in the paper. Dubovskii *et al.* (23) then used the plot of the chemical shift *versus* pH to determine the pK_a values of five Glu residues in the sequence, and Glu[11]

and Glu^{15} were shown to possess unusually high pK_a values of ~5.6 compared with a pK_a of 4.24 for isolated glutamic acid in aqueous solution. Based on these elevated pK_a values, the proposed model of Dubovskii *et al.* shows that fusion activity is likely driven by the protonation of the carboxylate group of the Glu^{11} residue participating in a transient hydrogen bond with the backbone amide proton of Glu^{15}. According to the model, once the side chain carboxylate of Glu^{11} is protonated at acidic pH (pH < 6), the fusion peptide relocates into the hydrophobic core of the micelle followed by stabilization of the amphipathic α-helix in residues 2–18. Interestingly, we found that the pK_a values of five Glu residues in the sequence (Glu^4, Glu^8, Glu^{11}, Glu^{15}, and Glu^{19}) of E5 and G13L peptides in SDS micelles are nearly identical to the values in DPC micelles reported by Dubovskii *et al.* This finding indicates that possessing unusual pK_a values in the Glu^{11} and Glu^{15} residues is not the only factor for the HA2 fusion peptide in fusion activity, because G13L is much less fusion-active than E5. In addition, we did not observe the hydrogen bond between the carboxylate group of Glu^{11} and the backbone H^N of Glu^{15} in our NMR structures of the E5 analog in SDS micelles. Apparently, the proposed model of Dubovskii *et al.* contradicts our biophysical data. In contrast, our model is similar to the one proposed by Han *et al.* (22). The solution structure of influenza HA2 host-guest fusion domain was determined to contain the structural motifs of helix-break-helix and helix-break-irregular at pH 5.0 and 7.4, respectively. Both structures are highly amphipathic and feature a bend in the middle, and this bend orients the two ends of the fusion domains toward their hydrophobic faces. Strikingly, the structural basis between native fusion peptide in DPC micelles and the E5 analog in SDS micelles at different pH values are almost identical. Because of the highly similar structural properties, our proposed model and that of Han *et al.* are alike.

In conclusion, all three models suggest that the N terminus from residues 2–11 exhibits a stable α-helix structure and that the fusion peptide possesses a higher helical content at acidic pH (fusogenic pH) than at neutral pH. Our E5 analog and the reported native fusion peptide NMR structures all showed a structural change in the C-terminal helix at different pH values. However, the importance of the hinge in the middle of the sequence and the C-terminal helix of HA2 fusion peptide in membrane fusion have not been reported before. In this work, our NMR data of G13L and L17A, as described above, directly demonstrate the importance of the hinge in Gly^{12}-Gly^{13} and the C-terminal 3_{10}-helix in Trp^{14}–Ile^{18} in fusion activity. It is known that the E5 analog and the native fusion peptide of influenza HA2 induce fusion activity at acidic pH and possess similar characteristics when interacting with the lipid bilayer. Most interestingly, we found that the structure/fusion activity relationships exhibited by the E5 analog represent well the property of the native fusion peptide of influenza virus HA2. Consequently, our model further provides insight into the mechanism of membrane fusion for influenza virus HA2 fusion peptide.

Acknowledgment—We thank Shu-Fang Cheng for performing acrylamide quenching experiments.

REFERENCES

1. Skehel, J. J., Bayley, P. M., Brown, E. B., Martin, S. R., Waterfield, M. D., White, J. M., Wilson, I. A., and Wiley, D. C. (1982) *Proc. Natl. Acad. Sci. U. S. A.* **79,** 968–972
2. White, J., Kartenbeck, J., and Helenius, A. (1982) *EMBO J.* **1,** 217–222
3. Wharton, S. A., Skehel, J. J., and Wiley, D. C. (1986) *Virology* **149,** 27–35
4. van Meer, G., Davoust, J., and Simons, K. (1985) *Biochemistry* **24,** 3593–3602
5. Macosko, J. C., Kim, C. H., and Shin, Y. K. (1997) *J. Mol. Biol.* **267,** 1139–1148
6. Haywood, A. M., and Boyer, B. P. (1985) *Proc. Natl. Acad. Sci. U. S. A.* **82,** 4611–4615
7. Midoux, P., Mayer, R., and Monsigny, M. (1995) *Biochim. Biophys. Acta* **1239,** 249–256
8. Luneberg, J., Martin, I., Nussler, F., Ruysschaert, J. M., and Herrmann, A. (1995) *J. Biol. Chem.* **270,** 27606–27614
9. Wilson, I. A., Skehel, J. J., and Wiley, D. C. (1981) *Nature* **289,** 366–373
10. Bullough, P. A., Hughson, F. M., Skehel, J. J., and Wiley, D. C. (1994) *Nature* **371,** 37–43
11. Barker, W. C., Garavelli, J. S., Haft, D. H., Hunt, L. T., Marzec, C. R., Orcutt, B. C., Srinivasarao, G. Y., Yeh, L. S. L., Ledley, R. S., Mewes, H. W., Pfeiffer, F., and Tsugita, A. (1998) *Nucleic Acids Res.* **26,** 27–32
12. Matsumoto, T. (1999) *Biophys. Chem.* **79,** 153–162
13. Lear, J. D., and DeGrado, W. F. (1987) *J. Biol. Chem.* **262,** 6500–6505
14. Murata, M., Takahashi, S., Shirai, Y., Kagiwada, S., Hishida, R., and Ohnishi, S. (1993) *Biophys. J.* **64,** 724–734
15. Gething, M. J., Doms, R. W., York, D., and White, J. (1986) *J. Cell Biol.* **102,** 11–23
16. Steinhauer, D. A., Wharton, S. A., Skehel, J. J., and Wiley, D. C. (1995) *J. Virol.* **69,** 6643–6651
17. Han, X., Steinhauer, D. A., Wharton, S. A., and Tamm, L. K. (1999) *Biochemistry* **38,** 15052–15059
18. Murata, M., Takahashi, S., Kagiwada, S., Suzuki, A., and Ohnishi, S. (1992) *Biochemistry* **31,** 1986–1992
19. Pichon, C., Freulon, I., Midoux, P., Mayer, R., Monsigny, M., and Roche, A. C. (1997) *Antisense Nucleic Acid Drug Dev.* **7,** 335–343
20. Brasseur, R., Vandenbranden, M., Cornet, B., Burny, A., and Ruysschaert, J. M. (1990) *Biochim. Biophys. Acta* **1029,** 267–273
21. Takahashi, S. (1990) *Biochemistry* **29,** 6257–6264
22. Han, X., Bushweller, J. H., Cafiso, D. S., and Tamm, L. K. (2001) *Nat. Struct. Biol.* **8,** 715–720
23. Dubovskii, P. V., Li, H., Takahashi, S., Arseniev, A. S., and Akasaka, K. (2000) *Protein Sci.* **9,** 786–798
24. Sreerama, N., and Woody, R. W. (1993) *Anal. Biochem.* **209,** 32–44
25. Lakowicz, J. R. (1983) *Principles of Fluorescence Spectroscopy*, Plenum Press, New York
26. Rance, M., Sorensen, O. W., Bodenhausen, G., Wagner, G., Ernst, R. R., and Wüthrich, K. (1983) *Biochem. Biophys. Res. Commun.* **117,** 479–485
27. Bax, A., and Davis, D. G. (1985) *J. Magn. Reson.* **65,** 355–360
28. Kumar, A., Ernst, R. R., and Wüthrich, K. (1980) *Biochem. Biophys. Res. Commun.* **95,** 1–6
29. Marion, D., and Wüthrich, K. (1983) *Biochem. Biophys. Res. Commun.* **113,** 967–974
30. Piotto, M., Saudek, V., and Sklenar, V. (1992) *J. Biomol. NMR* **2,** 661–665
31. Brunger, A. T. (1998) *X-PLOR*, Yale University Press, New Haven, CT
32. Koradi, R., Billeter, M., and Wüthrich, K. (1996) *J. Mol. Graph.* **14,** 29–32
33. Nicholls, A., Sharp, K. A., and Honig, B. (1991) *Proteins Struct. Funct. Genet.* **11,** 281–296
34. Laskowski, R. A., Rullmannn, J. A., MacArthur, M. W., Kaptein, R., and Thornton, J. M. (1996) *J. Biomol. NMR* **8,** 477–486
35. Creighton, T. E. (1993) *Proteins*, pp. 190–191, Freeman, New York
36. Rafalski, M., Ortiz, A., Rockwell, A., van Ginkel, L. C., Lear, J. D., DeGrado, W. F., and Wilschut, J. (1991) *Biochemistry* **30,** 10211–10220